RESEARCH ARTICLE | APRIL 09 2024

Retrieving positions of closely packed subwavelength nanoparticles from their diffraction patterns

Benquan Wang ; Ruyi An ; Eng Aik Chan ; Giorgio Adamo ; Jin-Kyu So ; Yewen Li ; Zexiang Shen ; Bo An ; Nikolay I. Zheludev

Appl. Phys. Lett. 124, 151105 (2024)
https://doi.org/10.1063/5.0194393

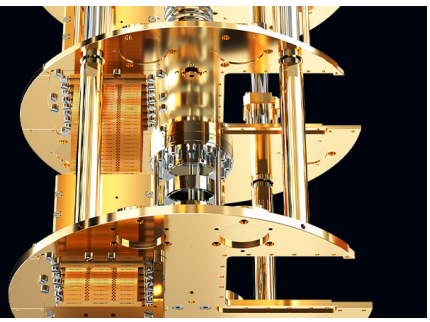

Retrieving positions of closely packed subwavelength nanoparticles from their diffraction patterns

Cite as: Appl. Phys. Lett. **124**, 151105 (2024); doi: 10.1063/5.0194393
Submitted: 10 January 2024 · Accepted: 25 March 2024 ·
Published Online: 9 April 2024

Benquan Wang,[1,2] Ruyi An,[3] Eng Aik Chan,[1,2,a)] Giorgio Adamo,[1,2] Jin-Kyu So,[1,2] Yewen Li,[3] Zexiang Shen,[1,2] Bo An,[3] and Nikolay I. Zheludev[1,2,4]

AFFILIATIONS

[1]Centre for Disruptive Photonic Technologies, TPI, Nanyang Technological University, 21 Nanyang Link, Singapore 637371, Singapore
[2]Division of Physics and Applied Physics, School of Physical and Mathematical Science, Nanyang Technological University, Singapore 637371, Singapore
[3]School of Computer Science and Engineering, Nanyang Technological University, Singapore 639798, Singapore
[4]Centre for Photonics Metamaterials and Optoelectronics Research Centre, University of Southampton, Southampton SO17 1BJ, United Kingdom

[a)]Author to whom correspondence should be addressed: echan003@e.ntu.edu.sg

ABSTRACT

Distinguishing two objects or point sources located closer than the Rayleigh distance is impossible in conventional microscopy. Understandably, the task becomes increasingly harder with a growing number of particles placed in close proximity. It has been recently demonstrated that subwavelength nanoparticles in closely packed clusters can be counted by AI-enabled analysis of the diffraction patterns of coherent light scattered by the cluster. Here, we show that deep learning analysis can return the actual positions of nanoparticles in the cluster. The Pearson correlation coefficient between the ground truth and reconstructed positions of nanoparticles exceeds 0.7 for clusters of ten nanoparticles and 0.8 for clusters of two nanoparticles of 0.16λ in diameter, even if they are separated by distances below the Rayleigh resolution limit of 0.68λ, corresponding to a lens with numerical aperture NA = 0.9.

Imaging, localization, and retrieval of the number of subwavelength objects closely packed, although extremely challenging, are problems that are very often encountered in applications, such as environmental monitoring,[1] semiconductor optical inspection,[2] materials,[3] and biomedical analysis.[4] This problem cannot be tackled by conventional microscopy, which is bound by the Abbe–Rayleigh diffraction limit to a resolution of about half the wavelength of the incident light. Improved resolution can be obtained by using optical techniques such as PALM and STED, which work with photoactivated labels[5–7] or near-field methods,[8,9] which require contact with the sample and are, therefore, unsuitable in many instances because of their complexity and invasiveness.[10]

It was recently reported that deep learning-enabled analysis of single-shot diffraction patterns of coherent light scattered by subwavelength objects can be used to obtain unlabeled super-resolution optical metrology[11,12] and to correctly predict the number of nano-objects in clusters of subwavelength objects.[13] Here, we show that AI-empowered analysis of the optical diffraction patterns of closely packed subwavelength nanoholes, using a neural network trained on similar *a priori* known objects, allows us to retrieve their positions, even when the nanoholes are touching.

We conducted numerical experiments using a coherent plane wave illumination ($\lambda = 633$ nm) of clusters of subwavelength nanoholes with a diameter of $\lambda/6.33$ perforated in an opaque film, randomly placed within a $2.2\ \lambda \times 2.2\ \lambda$ area. We image the diffraction patterns created by the nanoholes clusters at a distance, $H = 1\ \lambda$, away from the sample, over a $22\ \lambda \times 22\ \lambda$ field of view, accounting for the numerical aperture, NA = 0.9, of a real imaging system [Fig. 1(a)]. Pairs of the far-field diffraction pattern and the corresponding position map of nanoholes in the cluster were used to train a modified U-Net encoder–decoder convolutional neural network. U-Net is a convolutional neural network (CNN) architecture specifically designed for semantic image

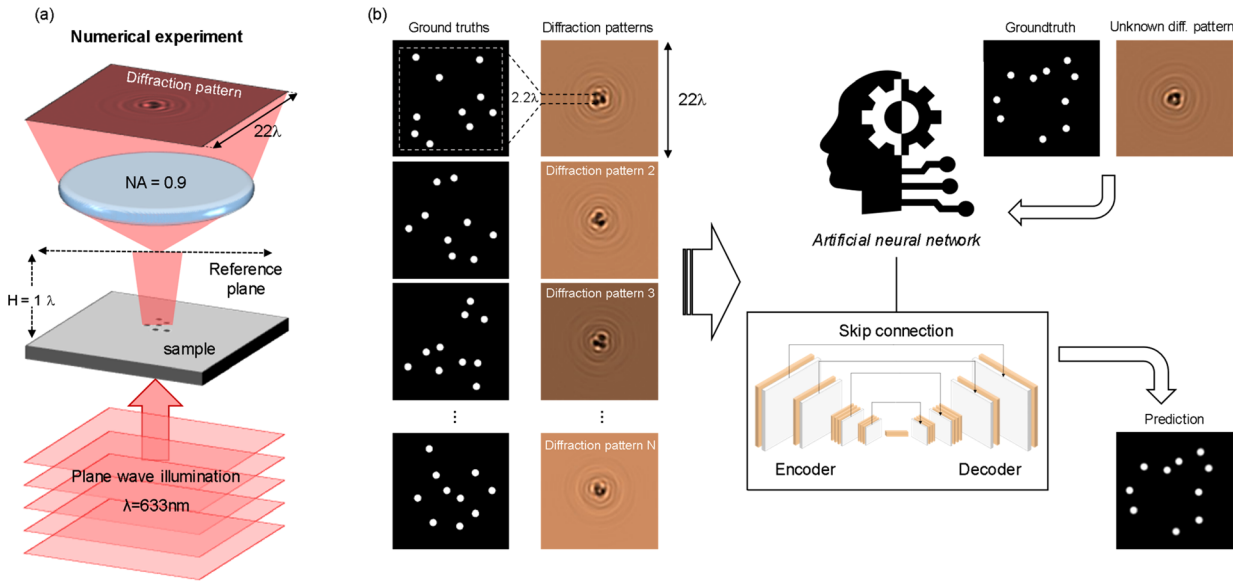

FIG. 1. (a) Schematic of the numerical experiment. Clusters of subwavelength nanoholes with diameters of $\lambda/6.33$, placed within a 2.2 $\lambda \times 2.2$ λ area in a 100 nm-thick chromium film, are illuminated by a plane wave with wavelength = 633 nm. The diffraction pattern of the scattered light intensity, at a distance, $H = 1\lambda$, is recorded with a numerical aperture, NA = 0.9. (b) Pairs of diffraction patterns and corresponding position maps of the nanoholes (ground truths) are used to train a modified U-Net, encoder–decoder convolutional neural network, which will then be able to retrieve the positions of nanoholes from single-shot unknown diffraction patterns.

segmentation,[14] i.e., categorizing each pixel in an image into a class or object, which continues to generate widespread interest and has found application in medical imaging[15] and optical microscopy.[16] The network has a U-shaped architecture consisting of an encoder, or dimension-reducing path, followed by a decoder or dimension-increasing path, with a symmetric design that reduces the risk of information loss during the encoding and decoding processes.[17] The encoder path captures and condenses information of inputs at multiple levels of abstraction through convolutional and pooling layers, as in traditional CNNs.[18] The decoder path, instead, uses transposed convolutions to recover the dimension, conditioned by skip connections from the correspondingly encoded information at the same level. This approach enables the network to produce precise segmentation masks and effectively addresses the vanishing gradient problem.[19] This phenomenon, where the network loses its capacity to capture long-term dependencies, is mitigated through this design. To promote efficient information propagation and resolve the category imbalance challenge in the particle localization problem (i.e., the small fraction of nanoholes with respect to the background), we modify the U-Net by introducing a residual architecture[20] with multiple deep convolutional layers and novel hybrid loss function that combines binary cross-entropy loss and a class-balanced loss (details are in the supplementary material Secs. 1–5). The trained network is then able to retrieve the positions of the particle in the cluster from previously unseen diffraction patterns [Fig. 1(b)].

Each sample contains up to 10 nanoholes that may form clusters with an inter-particle distance smaller than the Rayleigh limit of resolution of a conventional microscope, 0.61 λ/NA. We define the sizes of the sub-Rayleigh clusters by counting the number of nanoholes whose inter-particle distance is smaller than the Rayleigh limit [Fig. 2(a)] and characterize each sample by the largest sub-Rayleigh cluster size within the 2.2 $\lambda \times 2.2$ λ area. It shall be noted how, often, not only pairs but all particles fall within the Rayleigh distance [e.g., nanoholes A, B, and C in Fig. 2(a)]. The groundtruth maps used to supervise the network are binary images of 512 × 512 pixels size (corresponding to an area of 2.5 $\lambda \times 2.5$ λ), where white pixels (value = 1) represent the nanoholes and black pixels (value = 0) represent the Cr film [second column in Fig. 2(b)]. The corresponding diffraction patterns were generated plotting the total electric field intensity profiles calculated by finite-difference-time-domain (FDTD) full Maxwell solver (supplementary material Sec. 6), at a distance of 1 λ from the sample surface, over a field of view of 22 $\lambda \times 22$ λ [first column in Fig. 2(b)]. Figure 2(b) shows that the light propagating through the nanoholes generated very rich interference patterns in the diffraction maps, thus making it very difficult to correlate with a specific number and distribution of nanoholes on the sample. Nonetheless, the trained network can not only retrieve the number and positions of the nanoholes in the clusters but also return 512 × 512 pixels images [third column in Fig. 2(b)], where the sizes of the nanoholes match well those of the groundtruth and, therefore, can be regarded as a form of super-resolution imaging.

A total of 11 700 samples and corresponding diffraction patterns were generated for the numerical experiment, of which 7200 were used for training, 1800 for validation, and 2700 for testing (supplementary material Sec. 7). We use the Pearson correlation coefficient[21] between the predicted and ground truth images to evaluate the accuracy of image reconstruction of our technique,

$$r_{xy} = \frac{\sum_{i=1}^{n}(x_i - \bar{x})(y_i - \bar{y})}{\sqrt{\sum_{i=1}^{n}(x_i - \bar{x})^2}\sqrt{\sum_{i=1}^{n}(y_i - \bar{y})^2}}, \quad (1)$$

where n is the sample size and x_i and y_i are the individual sample points in our reconstructed image and ground truth image,

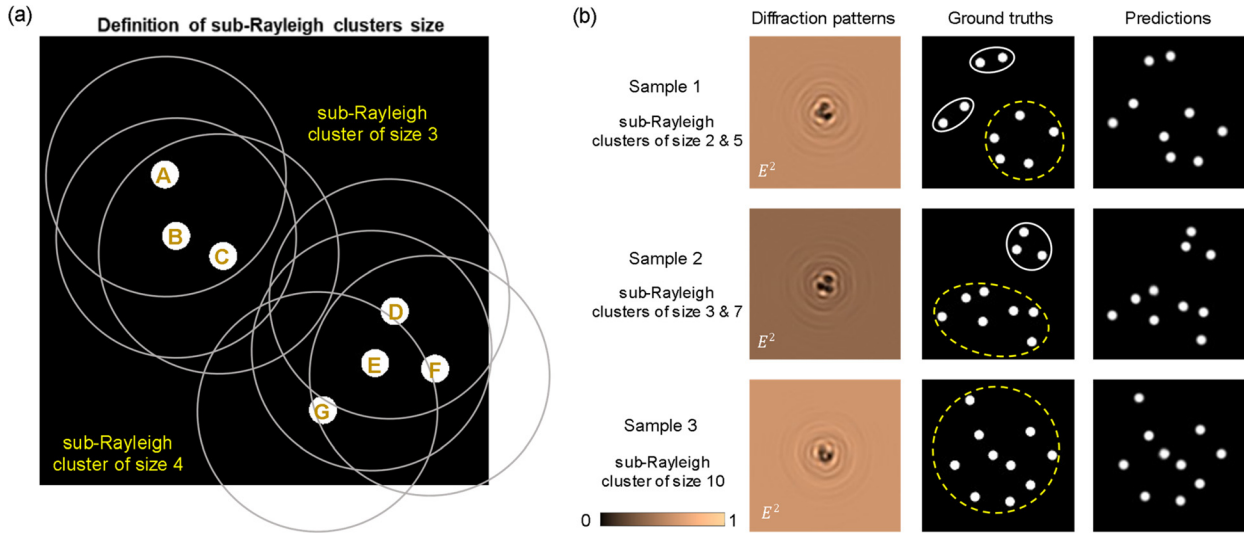

FIG. 2. (a) A group of nanoholes is identified as a sub-Rayleigh cluster if each nanohole in the cluster has at least one neighboring nanohole within Rayleigh distance, 0.61 λ/NA. The binary map shown here contains a sub-Rayleigh cluster of three nanoholes (A)–(C) and a cluster of four nanoholes (D)–(G). The circles represent the Rayleigh region of each nanohole. Nanoholes (A)–(C) and nanoholes (D)–(F) all fall within the Rayleigh distance. (b) Diffraction patterns (first column), groundtruth (second column), and prediction (third column) images of three samples where the size of the largest Rayleigh cluster (yellow dashed circle) increases from 5 (first row) to 7 (second row) and 10 (third row).

respectively, indexed with i, $\bar{x} = \frac{1}{n}\sum_{i=1}^{n} x_i$ (the sample mean), and analogously for $\bar{y}$.

Figure 3(a) shows that the accuracy exceeds 0.81 for samples with the sub-Rayleigh cluster index of 3 and remains as high as 0.71 for samples containing ten nanoholes within the same sub-Rayleigh cluster, which is an indication of the trained network's robustness against the size of sub-Rayleigh clusters. The decrement of the image reconstruction accuracy with the increasing size of sub-Rayleigh clusters can be justified by the increase in the complexity of the interference patterns.

To explore further our technique and test its resilience against the problem of closely paced particles, we tested its performance with an example of two closely spaced nanoholes. In this case, we use 800 diffraction patterns of two λ/6.33 nanoholes with center-to-center separation decreasing from 0.677 λ (Rayleigh distance) to 0.158 λ (touching) as a test. The Pearson correlation coefficient calculated in Fig. 3(b) shows that the two nanoholes could be resolved with an accuracy higher than 0.8 across almost the entire range of sub-Rayleigh distances, with a slight drop to 0.75 in the only case of touching nanoholes.

In conclusion, we report on a far-field, single-shot super-resolution optical technique based on the deep learning of the light diffracted on the clusters of subwavelength particles. It allows retrieving maps showing the number, positions, and sizes of the nanoparticles in the cluster and, therefore, constitutes a form of imaging. Our technique

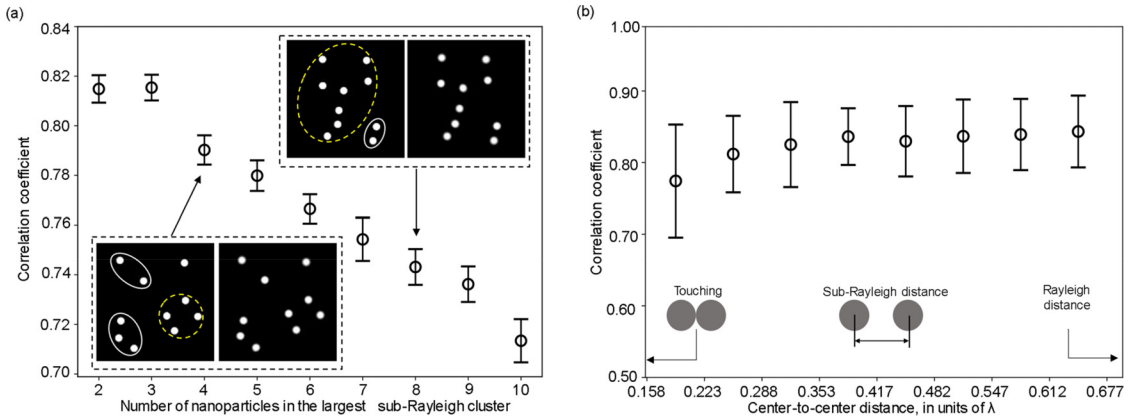

FIG. 3. (a) Pearson correlation coefficient between the predicted and ground truth images as a function of the sub-Rayleigh cluster size. Insets: examples of groundtruth (left) and prediction (right) images for samples with the largest sub-Rayleigh cluster size of 4 (lower left) and 8 (upper right) nanoholes. (b) Pearson correlation coefficient between the predicted and ground truth images for the typical Rayleigh diffraction case, two closely spaced nanoholes of decreasing center-to-center distance.

is scalable to different wavelengths and film materials as long as the film material is opaque for the wavelength. The image reconstruction accuracy measured as the correlation coefficient between the ground truth and reconstructed maps of the nanoparticles depends on the number of nanoparticles in the largest cluster of sub-Rayleigh spaced particles and varies from 0.82 to 0.71 when the cluster size increases from 2 to 10. In addition, we showed that the technique resolves nanoholes separated significantly smaller than the Rayleigh distance.

See the supplementary material for details on the network (architecture, optimization objectives, hyperparameters, and tailored objective functions) and the dataset distribution used for training, numerical simulations, and performance with noise.

This work was supported by the Singapore National Research Foundation (Grant No. NRF-CRP23-2019-0006), the Singapore Ministry of Education (Grant No. MOE2016-T3-1-006), and the Engineering and Physical Sciences Research Council UK (Grants No. EP/T02643X/1).

AUTHOR DECLARATIONS

Conflict of Interest

The authors have no conflicts to disclose.

Author Contributions

Benquan Wang: Conceptualization (lead); Data curation (lead); Formal analysis (equal); Investigation (equal); Methodology (lead); Software (equal); Validation (lead); Visualization (lead); Writing – original draft (equal); Writing – review & editing (equal). **Ruyi An:** Formal analysis (equal); Software (equal); Validation (supporting); Visualization (supporting); Writing – review & editing (equal). **Eng Aik Chan:** Formal analysis (equal); Investigation (equal); Project administration (lead); Software (equal); Writing – review & editing (equal). **Giorgio Adamo:** Formal analysis (equal); Investigation (equal); Visualization (equal); Writing – original draft (equal); Writing – review & editing (equal). **Jin-Kyu So:** Formal analysis (equal); Investigation (equal); Visualization (equal); Writing – original draft (equal); Writing – review & editing (equal). **Yewen Li:** Formal analysis (equal); Investigation (equal); Software (equal); Writing – review & editing (equal). **Zexiang Shen:** Funding acquisition (equal); Resources (equal); Supervision (equal); Writing – review & editing (equal). **Bo An:** Funding acquisition (equal); Supervision (equal); Writing – review & editing (equal). **Nikolay I. Zheludev:** Funding acquisition (lead); Resources (lead); Supervision (lead); Writing – review & editing (equal).

DATA AVAILABILITY

The data that support the findings of this study are available from the corresponding author upon reasonable request.

REFERENCES

[1]C. Dincer, R. Bruch, E. Costa-Rama, M. T. Fernández-Abedul, A. Merkoçi, A. Manz, G. A. Urban, and F. Güder, Adv. Mater. **31**(30), 1806739 (2019).
[2]S. Purandare, J. Zhu, R. Zhou, G. Popescu, A. Schwing, and L. L. Goddard, Opt. Express **27**(13), 17743 (2019).
[3]S. Pujals, N. Feiner-Gracia, P. Delcanale, I. Voets, and L. Albertazzi, Nat. Rev. Chem. **3**(2), 68 (2019).
[4]L. Schermelleh, A. Ferrand, T. Huser, C. Eggeling, M. Sauer, O. Biehlmaier, and G. P. C. Drummen, Nat. Cell Biol. **21**(1), 72 (2019).
[5]S. W. Hell and J. Wichmann, Opt. Lett. **19**(11), 780 (1994).
[6]M. J. Rust, M. Bates, and X. Zhuang, Nat. Methods **3**(10), 793 (2006).
[7]E. Betzig, G. H. Patterson, R. Sougrat, O. W. Lindwasser, S. Olenych, J. S. Bonifacino, M. W. Davidson, J. Lippincott-Schwartz, and H. F. Hess, Science **313**(5793), 1642 (2006).
[8]R.-H. Jiang, C. Chen, D.-Z. Lin, H.-C. Chou, J.-Y. Chu, and T.-J. Yen, Nano Lett. **18**(2), 881 (2018).
[9]D. P. Tsai and W. C. Lin, Appl. Phys. Lett. **77**(10), 1413 (2000).
[10]V. N. Astratov, Y. Ben Sahel, Y. C. Eldar, L. Huang, A. Ozcan, N. Zheludev, J. Zhao, Z. Burns, Z. Liu, E. Narimanov, N. Goswami, G. Popescu, E. Pfitzner, P. Kukura, Y. Hsiao, C. Hsieh, B. Abbey, A. Diaspro, A. Legratiet, P. Bianchini, N. T. Shaked, B. Simon, N. Verrier, M. Debailleul, O. Haeberlé, S. Wang, M. Liu, Y. Bai, J. Cheng, B. S. Kariman, K. Fujita, M. Sinvani, Z. Zalevsky, X. Li, G. Huang, S. W. Chu, O. Tzang, D. Hershkovitz, O. Cheshnovsky, M. J. Huttunen, S. G. Stanciu, V. N. Smolyaninova, I. I. Smolyaninov, U. Leonhardt, S. Sahebdivan, Z. Wang, B. Luk'Yanchuk, L. Wu, A. V. Maslov, B. Jin, C. R. Simovski, S. Perrin, P. Montgomery, and S. Lecler, Laser Photonics Rev. **17**(12), 2200029 (2023).
[11]C. Rendón-Barraza, E. A. Chan, G. Yuan, G. Adamo, T. Pu, and N. I. Zheludev, APL Photonics **6**(6), 066107 (2021).
[12]T. Pu, J. Y. Ou, V. Savinov, G. Yuan, N. Papasimakis, and N. I. Zheludev, Adv. Sci. **8**(1), 2002886 (2021).
[13]E. A. Chan, C. Rendón-Barraza, B. Wang, T. Pu, J.-Y. Ou, H. Wei, G. Adamo, B. An, and N. I. Zheludev, Nanophotonics **12**(14), 2807–2812 (2023).
[14]O. Ronneberger, P. Fischer, and T. Brox, in *18th International Conference on Medical Image Computing and Computer-Assisted Intervention (MICCAI)* (Springer International Publishing, 2015), pp. 234–241.
[15]S. He, R. Bao, P. E. Grant, and Y. Ou, arXiv:2304.01401 (2023).
[16]X. Chen, M. E. Kandel, S. He, C. Hu, Y. J. Lee, K. Sullivan, G. Tracy, H. J. Chung, H. J. Kong, M. Anastasio, and G. Popescu, Nat. Photonics **17**(3), 250 (2023).
[17]W. Zhang, Z. Zhang, L. Bian, H. Wang, J. Suo, and Q. Dai, Opt. Lett. **46**(21), 5477 (2021).
[18]J. Gu, Z. Wang, J. Kuen, L. Ma, A. Shahroudy, B. Shuai, T. Liu, X. Wang, G. Wang, J. Cai, and T. Chen, Pattern Recognit. **77**, 354 (2018).
[19]S. Hochreiter, Int. J. Uncertainty, Fuzziness Knowl.-Based Syst. **6**(2), 107 (1998).
[20]K. He, X. Zhang, S. Ren, and J. Sun, in *IEEE Conference on Computer Vision and Pattern Recognition (CVPR)* (IEEE, 2016), pp. 770–778.
[21]J. A. Rice, *Mathematical Statistics and Data Analysis*, 3rd ed. (Thomson/Brooks/Cole, Belmont, CA, 2007).